

GPIP: Geometry-enhanced Pre-training on Interatomic Potentials

Taoyong Cui^{1,2†}, Chenyu Tang^{1,3,4†}, Mao Su^{1*}, Shufei Zhang^{1*},
Yuqiang Li¹, Lei Bai¹, Yuhan Dong², Xingao Gong^{5,6},
Wanli Ouyang¹

¹Shanghai Artificial Intelligence Laboratory, Shanghai, 200232, China.

²Shenzhen International Graduate School, Tsinghua University, Shenzhen, 518055, China.

³CAS Key Laboratory of Theoretical Physics, Institute of Theoretical Physics, Chinese Academy of Sciences, Beijing, 100190, China.

⁴School of Physical Sciences, University of Chinese Academy of Sciences, Beijing, 100049, China.

⁵Key Laboratory for Computational Physical Sciences (MOE), State Key Laboratory of Surface Physics, Department of Physics, Fudan University, Shanghai, 200433, China.

⁶Shanghai Qi Zhi Institute, Shanghai, 200232, China.

*Corresponding author(s). E-mail(s): sumao@pjlab.org.cn;
zhangshufei@pjlab.org.cn;

[†]These authors contributed equally to this work. This work was done during their internship at Shanghai Artificial Intelligence Laboratory.

Abstract

Machine learning interatomic potentials (MLIPs) enables molecular dynamics (MD) simulations with ab initio accuracy and has been applied to various fields of physical science. However, the performance and transferability of MLIPs are limited by insufficient labeled training data, which require expensive ab initio calculations to obtain the labels, especially for complex molecular systems. To address this challenge, we design a novel geometric structure learning paradigm that consists of two stages. We first generate a large quantity of 3D configurations of target molecular system with classical molecular dynamics simulations. Then, we propose geometry-enhanced self-supervised learning consisting of masking, denoising, and contrastive learning to better capture the topology and 3D

geometric information from the unlabeled 3D configurations. We evaluate our method on various benchmarks ranging from small molecule datasets to complex periodic molecular systems with more types of elements. The experimental results show that the proposed pre-training method can greatly enhance the accuracy of MLIPs with few extra computational costs and works well with different invariant or equivariant graph neural network architectures. Our method improves the generalization capability of MLIPs and helps to realize accurate MD simulations for complex molecular systems.

Keywords: Pre-train, Interatomic Potential, Graph Neural Network

1 Introduction

Molecular Dynamics (MD) simulation provides atomic insights in many areas such as physics, chemistry, biology, and material science [1–4]. The accuracy and efficiency of MD simulations depend on the choice of interatomic potentials, which are mathematical functions that describe the potential energy of atoms in a molecular system. In classical MD (CMD) simulations, the interatomic potentials are modeled by empirical formula with parameters to be fitted [5]. The CMD simulations are computationally efficient but inaccurate for many applications, especially those involving chemical reactions. In ab initio MD (AIMD) simulations, the interatomic potentials are accurately determined by solving Schrodinger’s equation [6]. However, the computational cost of AIMD is not affordable to simulate large systems. Machine learning interatomic potentials (MLIPs) are promising alternatives that can achieve ab initio level accuracy with high efficiency by using machine learning models to fit the ab initio energies and forces [7–9]. Among them, Graph Neural Networks (GNNs) are widely used by learning the interatomic potential directly from the atomic coordinates and chemical symbols without relying on any predefined functional form or prior knowledge [10]. GNNs can also leverage physical systems’ inherent symmetries and invariances, such as translation, rotation, and permutation, to improve their performance [11, 12]. Equivariant neural networks have also been developed to preserve the equivariance of molecular systems to improve the performance of interatomic potential predictions [13–17].

Although MLIPs have been extensively studied, their performance and transferability are still limited by the scarcity of training data due to expensive ab initio calculations. Various self-supervised learning (SSL) pre-training approaches have been explored to learn transferable representations from abundant unlabeled data [18–21]. The pre-trained model is then fine-tuned to extract more task-specific information from the limited supervised data. Three types of SSL approaches are widely studied including generation-based method [21–28], auxiliary property classification [29–33], and contrastive learning [34–39]. While some of those methods are applied in molecular property prediction, only a few works investigate the pre-training methods for the task of MD simulations, including the supervised pre-training method [40] and the self-supervised pre-training method [41]. These pre-training methods rely on existing datasets generated by expensive ab initio calculations such as OC20 [42] (catalytic

systems) and ANI-1 [43] (small molecules), which are unscalable due to the expensive cost in generating sufficient pre-training data with ab initio calculations and have limited generalization ability to new molecular systems that are not covered by the existing datasets.

In this work, we advocate a new learning paradigm by first conducting self-supervised pre-training on the cheap and easy-to-obtain CMD data [5] and then fine-tuning on the labeled data generated by AIMD to learn the task-related information. Under this paradigm, large-scale pre-training datasets can be easily generated with limited cost for a specific molecular system, enhancing the pre-training ability and avoiding the domain gap between the systems of pre-training data and test data. Besides, we also propose a geometry-enhanced self-supervised learning that involves three complementary tasks, including restoring the masked atoms with noisy coordinates, predicting noise with the masked atoms [41], and contrastive learning with 3D network [39] to better extract topology and 3D geometric information from CMD data. We demonstrate that the CMD structures without labels benefit interatomic potential predictions. To prove the effectiveness of our method, we pre-train MLIPs with GPIIP and apply them to various challenging benchmarks for interatomic potential prediction. To better evaluate the capability of MLIPs, we also develop an electrolyte solution dataset that includes many more types of elements and configurations. We emphasize that the computational complexity of GPIIP is negligible compared to ab initio calculations for obtaining accurate labels for the training set. Although increasing the number of training data can also improve accuracy, the computational cost will be thousands of times higher than GPIIP.

We list the main contributions: (1) We propose a novel geometric learning paradigm for MLIPs, GPIIP, consisting of two components: geometric structure generation and geometry-enhanced pre-training. (2) We demonstrate that the unlabeled geometric structures produced by CMD simulations benefit interatomic potential predictions with very small computational costs. (3) We design a geometry-enhanced self-supervised pre-training method for molecular structural data. (4) We evaluate our method using various MLIPs and datasets covering various molecular systems. Our method shows consistent and robust performance in all the experiments.

2 Results

In this section, the preliminary knowledge for modeling molecules with GNNs is first introduced. Then we present the details of the GPIIP framework. Finally, our experimental results on various molecular datasets are discussed.

2.1 Preliminaries

A certain molecule conformation can be uniquely represented by n atoms with atomic numbers $Z = (z_1, \dots, z_n)$ and atomic positions $R = (r_1, \dots, r_n)$. The atom features are first initialized using embedding: $X^0 = A_Z$ where $X^0 = (x_1^0, \dots, x_n^0)$ and $A_Z = (a_{z_1}, \dots, a_{z_n})$. The atom embeddings $\{a_{z_i}\}_{i=1}^n$ are randomly initialized and updated during training. Then, the graph neural network is used to further iteratively update the atom features through the message-passing schemes:

$$m_{ij}^l = f_m^l(x_i^l, x_j^l, \alpha_{ij}) \quad (1)$$

where α_{ij} represents the interaction between atoms i and j (usually, it is the distance or adjacency between atoms i and j), x_i^l and x_j^l are features for atoms i and j respectively at the l^{th} layer. Next, the messages $\{m_{ij}^l\}_{j \in \mathcal{N}_i}$ at the l^{th} layer from neighbors \mathcal{N}_i of atom i are aggregated and the corresponding atom feature is updated by the function f_u^l :

$$x_i^{l+1} = f_u^l(x_i^l, \sum_{j \in \mathcal{N}_i} m_{ij}^l). \quad (2)$$

Finally, the updated features are leveraged in various downstream tasks, such as predicting the system energy and atom forces.

In this work, we implement our proposed GPIIP on two invariant GNNs (SchNet [11] and SphereNet [44]) and three equivariant baseline models (EGNN [17], GemNet-T [45] and PaiNN [46]) to prove its effectiveness. The selected baseline models handle unevenly spaced data (i.e., atoms at arbitrary positions) and use different message-passing schemes to predict energies and forces. These models also cover a wide range of invariant/equivariant GNNs and exhibit competitive performance on various interatomic potential benchmarks.

2.2 GPIIP framework

Overview of GPIIP

In this paper, we present GPIIP, a novel geometric structure learning paradigm that leverages low-cost structural data to learn richer configuration information. First, structural data of target molecular systems are generated by CMD simulations with empirical force fields. Next, we only use the 3D configurations for pre-training to learn both topology and spatial structure information. We note that, for complex molecular systems with periodic boundary conditions (PBCs), a single pre-training task cannot effectively learn the good structure representations of molecules. Therefore, we propose geometry-enhanced self-supervised learning that consists of two complementary pre-training tasks: restoring the masked atoms with noisy coordinates, predicting noise with the masked atoms [41], and contrastive learning with 3D Nets. Our method is model-agnostic which can be implemented on different types of GNNs. The overall architecture of GPIIP is illustrated in Figure 1.

CMD simulations with empirical force fields

Empirical force fields are widely used in CMD simulations because they are computationally efficient and can handle large and complex systems. Despite the limitations such as accuracy and transferability compared with ab initio methods, CMD simulations can provide abundant structural information useful to improve the performance of MLIPs. There are force field models that cover most of the periodic table, such as the universal force field (UFF) [47] and the all-atom optimized potentials for liquid simulations (OPLS-AA) force field [5]. In this work, we perform CMD simulations of our target molecular systems using the OPLS-AA force field to generate large molecular geometry datasets for pre-training tasks.

Restore the Masked Atoms with Noisy Coordinates.

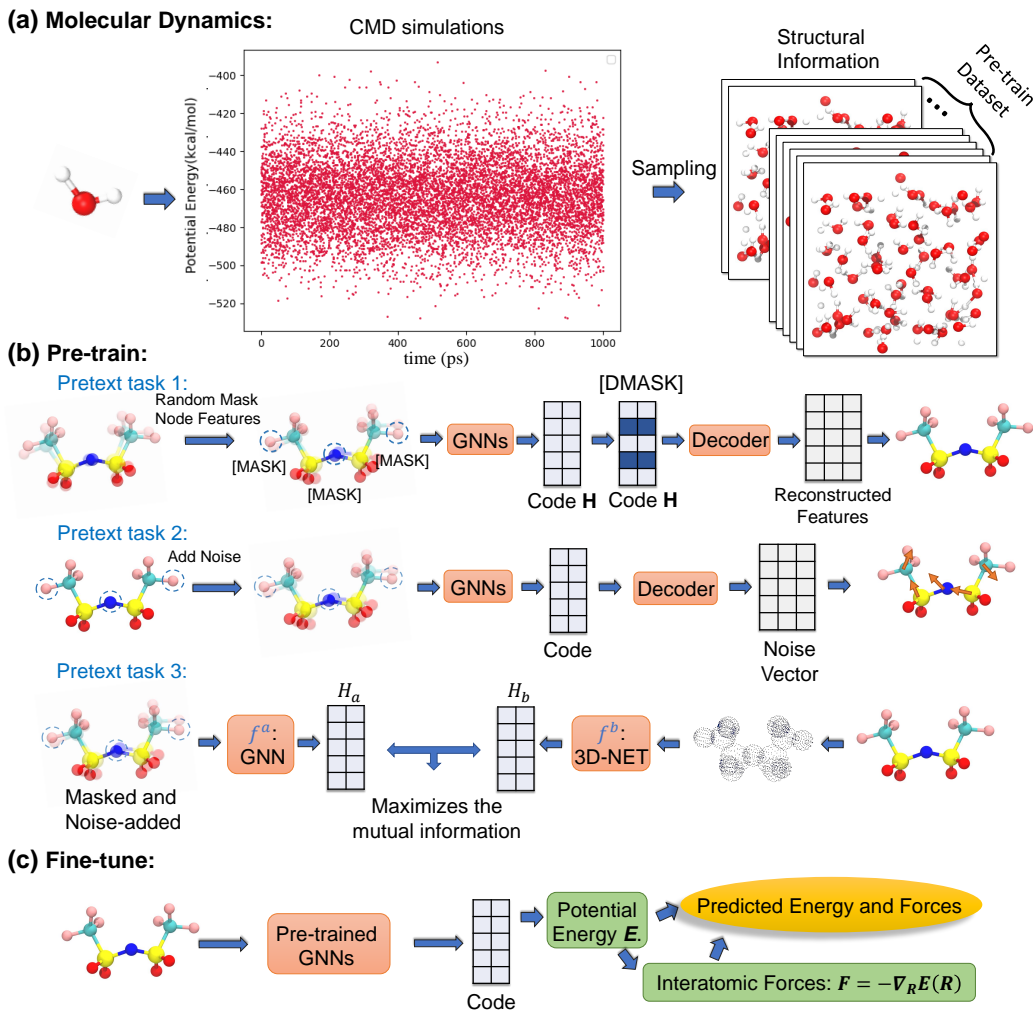


Fig. 1 The overall workflow. (a) CMD simulations are performed to generate datasets for pre-training. The structural data are sampled from simulation trajectories. (b) The pre-training part contains three complementary pretext tasks: masked atom restoration with noisy coordinates, noise prediction with masked atoms, and contrastive learning with 3D Nets. (c) GNNs are fine-tuned using labeled data after pre-training.

We adopt a masking mechanism to enhance the ability of GNNs to capture the topology information in molecular graphs. As a ground-breaking self-supervised paradigm for pre-training, the Masked Autoencoders [48] achieves state-of-the-art on various downstream tasks in the field of computer vision and natural language processing. By learning the representations of masked atoms via global interpolation of visible atoms, Masked Autoencoders can capture the topology information that what atoms are close to or connected with each other. If we know such the proximity relationship among

atoms, it will make it easier for us to predict the force exerted on atoms in downstream tasks. The masking task process is illustrated in Pretext task 1 of Figure 1. We first sample a subset of nodes \tilde{N} and mask their features with a mask token [MASK]. Then we use the GNN encoder to convert the masked conformation into a latent code \mathbf{H} and attempt to restore the masked features of the nodes in \tilde{N} with the decoder, based on the partially observed node signals and atom coordinates. To prevent the trivial solution of GNN encoder caused by atom-type information leakage via 3D coordinates and learn more useful topology information, we add the small noise to atom coordinates and leverage the re-mask technique on latent code \mathbf{H} (we replace the feature vectors of masked node indices in \mathbf{H} with another mask token [DMASK]) [23]. To avoid bias from predicting a fixed set of masked nodes that may not represent the whole graph structure, we use a uniform sampling strategy to select the nodes to mask that can cover the whole graph. Furthermore, the [MASK] token may lead to a discrepancy between training and inference, as it is absent during inference. Therefore, we replace the [MASK] token with a random token with a low probability (e.g., 15% or less). During training, we use the scaled cosine error as the criterion for reconstructing original node features which eliminates the effect of dimensionality and vector norms, allowing for more accurate reconstructions.

Predict Noise with the Masked Atoms.

To extract the spatial structure information of atoms, we leverage denoising autoencoders (DAEs) [49] to pre-train GNNs. By purifying the noisy version of the input, DAE can help to capture atomic position information of the pre-training data. As shown in Pretext task 2 of Figure 1, we perturb the molecular conformation by adding the random noise $\mathcal{E} \in \mathbb{R}^{n \times 3}$ drawn from a Gaussian distribution to the coordinates of each atom. The coordinates of perturbed conformation are denoted as $\hat{R} = R + \mathcal{E}$. We then train an autoencoder $g_\phi \circ f_\theta$ to minimize the reconstruction error $\|g_\phi(f_\theta(\tilde{X}^0, \hat{R})) - \mathcal{E}\|^2$ where \tilde{X}^0 represent the features of masked atoms. The encoder f_θ and decoder g_ϕ are parameterized by two sets of trainable parameters θ and ϕ . The standard denoising autoencoder objective is to predict the noiseless coordinates R . However, GNNs with skip connections can easily restore R from \hat{R} , which can not capture useful spatial information. Therefore, we opted to predict the noise vector \mathcal{E} directly instead of predicting the noiseless R . To make this task more challenging, we randomly sampled a certain proportion of nodes and masked their features. The magnitude of noise added to the conformations is a crucial hyperparameter in denoising pre-training. The noise variance σ should be large enough to force the GNNs to learn the meaningful spatial structures representation, but not so large that causes excessive distribution shift between clean and noisy conformations.

Contrastive Learning with 3D Network.

To further extract the global 3D information from the molecule conformations, we use contrastive learning to enforce GNN to learn the representations of a 3D network. The 3D network encodes the pairwise Euclidean distances among all atoms which can completely describe the 3D conformation. Therefore, the 3D network is deemed to be able to capture more 3D geometric information and long-range interactions.

As shown in Pretext task 3 of Figure 1, we feed the perturbed molecule conformation into GNN f^a and generate the latent code \mathbf{H}_a . Meanwhile, the 3D network f^b transforms

Table 1 Dataset summary. #Atoms: number of atoms in each sample. #Pre-train: number of samples used for pre-training. #Fine-tune: number of samples used for fine-tuning.

Dataset	System Type	PBC	#Atoms	#Pre-train	#Fine-tune
MD17	Small molecule	✗	9-21	160k	1k
ISO17	Isomers of C ₇ O ₂ H ₁₀	✗	19	2000k	20k/400k
Water	liquid	✓	192	100k	10k/1k
Electrolyte	liquid solution	✓	288-480	300k	1k/0.3k

the atoms’ coordinates to the pairwise Euclidean distances of all atoms and maps them to a higher dimensional space using sine and cosine functions. Then, such features are converted into latent code \mathbf{H}_b .

Next, we maximize the mutual information between the output features of GNN f^a and 3D network f^b . In such a way, as the main prediction network, GNN f^a can learn more 3D information from 3D network f^b which can help improve downstream interatomic potential predictions. Pretext task 3 can also be seen as a contrastive distillation process, where the student GNN learns from the teacher 3D network to capture the 3D information.

2.3 Experiments

We evaluate the performance of GPIP on multiple benchmark datasets ranging from simple systems (MD17 [50], ISO17 [11]) to complex systems with PBCs (liquid water [51] and our new dataset of electrolyte solutions), as shown in Figure 2 and Table 1. In all these experiments, the datasets for pre-training are generated by CMD simulations and the datasets for fine-tuning are generated by ab initio methods.

MD17: MD Trajectories of small molecules

The MD17 dataset consists of MD trajectories of small organic molecules with reference values of energy and forces calculated by ab initio molecular dynamics (AIMD) simulations. The training and validation sets consist of a combined 1,000 configurations. We use a pre-training dataset of 160,000 configurations sampled from CMD trajectories of eight different organic molecules. The results of GPIP-based models compared with baseline models are listed in Table 2. It is clear that the performances of GPIP-based SchNet and SphereNet are better than their corresponding baseline models. Especially, the performance of SphereNet-GPIP surpasses NequIP [14], the state-of-the-art MLIP, for all molecules in the MD17 dataset. We also perform several ablation studies to study the effect of each task in GPIP and the results are summarized in Supplementary Material.

ISO17: MD Trajectories of C₇O₂H₁₀ isomers

The ISO17 dataset [52] consists of MD trajectories of C₇O₂H₁₀ isomers generated by AIMD simulations. The pre-training dataset consists of 2,000,000 configurations sampled from CMD trajectories with a time resolution of 1 ps. The original ISO17 dataset is used for fine-tuning. We use a smaller dataset of 20,000 configurations and a larger dataset of 400,000 configurations respectively for fine-tuning. Two different settings are considered here to evaluate the generalization of MLIPs across conformational space. For the unknown molecules/unknown conformations task, the molecules in the

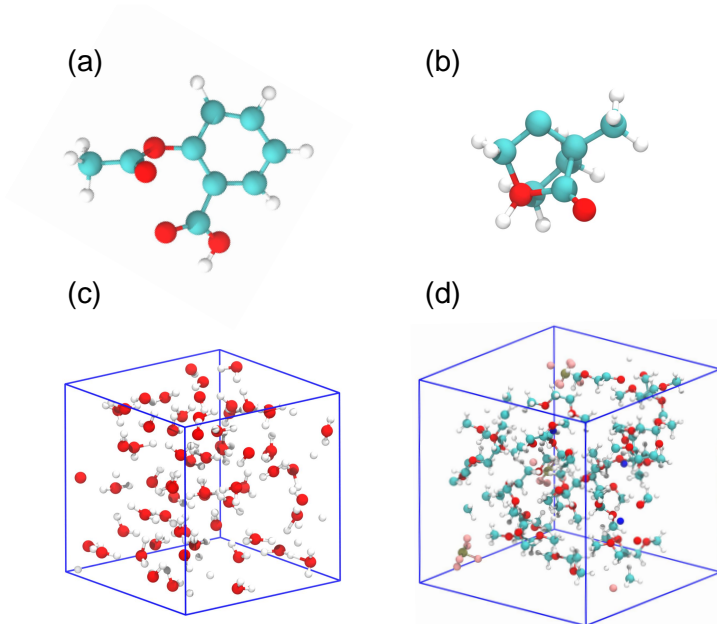


Fig. 2 Visualization of the atomic structures in benchmark systems. (a) An aspirin molecule from MD17 dataset. (b) A C₇O₂H₁₀ molecule in the ISO17 dataset. (c) A snapshot of liquid water with PBCs. (d) A snapshot of electrolyte solution ([Na]⁺+ [PF₆]⁻+DME) with PBCs.

Table 2 Results on MD17 dataset. MAE of forces (F) are shown in the unit of [kcal/mol/Å]. Results of all baseline models are directly taken or adapted (if the unit varies) from the original papers. The weights of force over energy in loss functions are set to 100 in line with the original papers of the different baselines for fair comparisons. The best results are shown in bold.

		NequIP [14]	SchNet [11]	SchNet-GPIP	SphereNet [44]	SphereNet-GPIP
Aspirin.	F	0.353	1.35	0.85	0.430	0.301
Benzene.	F	0.186	0.31	0.27	0.178	0.155
Ethanol.	F	0.204	0.39	0.27	0.208	0.150
Malonaldehyde.	F	0.328	0.66	0.53	0.340	0.261
Naphthalene.	F	0.105	0.58	0.45	0.178	0.093
Salicylic acid.	F	0.242	0.85	0.58	0.360	0.204
Tolunene	F	0.102	0.57	0.41	0.155	0.090
Uracil	F	0.173	0.56	0.48	0.267	0.195
std. MAE	F	0.79	2.38	1.08	0.97	0.70

validation set are not in the training set. As shown in Table 3, GPIP-based MLIPs significantly outperform their non-pre-trained counterparts on both tasks, even though the training set is very large.

We also evaluate the effect of GPIP with various amounts of training data. The training data are randomly sampled from the original training set while the validation and test sets remain unchanged. Figure 3 shows the results of force predictions with

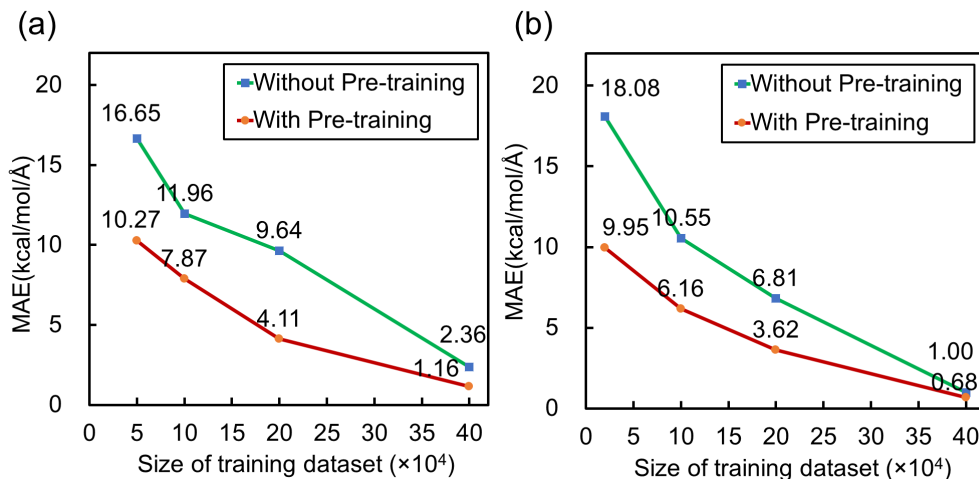


Fig. 3 MAEs of forces of EGNN (a) and SchNet (b) with different amount of training data on the ISO17 dataset.

EGNN and SchNet. The GPIP-based MLIPs perform better than the non-pre-trained counterpart throughout the experiments. We find that using only 10,000 training data, the GPIP-based SchNet achieves an MAE of 9.95, much lower than the non-pre-trained SchNet with an MAE of 18.08. This performance is even better than the non-pre-trained SchNet trained using 10 times more training data (10.55). Therefore, we demonstrate that GPIP-based MLIPs are more data efficient than those trained from scratch in achieving comparable performance. Although the MAE continues to decline with increasing training data, considering the computational costs for acquiring high-precision labeled training data, GPIP can achieve comparable accuracy with far fewer computational resources. For example, the GPIP-based SchNet achieves an MAE of 6.16 with 100,000 training data, while the non-pre-trained SchNet achieves an MAE of 6.81 with 200,000 training data. Using GPIP, the additional computational costs include 60 CPU core hours for CMD data generation and 5 minutes of GPU computation (using one NVIDIA A100 card) for pre-training. In comparison, obtaining an additional 100,000 labeled ISO17 data by ab initio calculation requires about 53,000 CPU core hours.

Liquid Water with PBCs

The extended systems with PBCs are more difficult for SSL methods due to their structural complexity. Water is arguably the most important molecular liquid in biological and chemical processes, and its complex thermodynamic and phase behaviors pose great challenges for computational studies. The liquid water dataset used for pre-training is generated by CMD with 100,000 configurations calculated at 10 different temperatures ranging from 100 K to 1000 K. The dataset used for fine-tuning is collected every 10 fs from a 1 ns trajectory sampled at equilibrium with a temperature of 300 K. For SchNet, we use 9,500 and 500 data for training and validation, respectively.

Table 3 Results on ISO17 (C₇O₂H₁₀ isomers) dataset. MAEs for energy and force are reported in [kcal/mol] and [kcal/mol/Å], respectively.

		SchNet		SchNet-GPIP	
		20,000 data	400,000 data	20,000 data	400,000 data
known molecules / unknown conformation	Energy	17.81	0.36	8.93	0.24
	Force	18.08	1.00	9.95	0.68
unknown molecules / unknown conformation	Energy	17.73	2.40	9.89	1.29
	Force	17.63	2.18	10.12	1.70

Table 4 Results on Water dataset. The force MAE is reported in the unit of [meV/Å], stability is reported in the unit of [ps], and RDF MAE is unitless. Diffusivity is computed by averaging 5 runs from 5 random initial configurations and its MAE is reported in the unit of [10^{-9} m²/s]. The number inside the parentheses represents the standard deviation from 5 simulations. The stable trajectory of GemNet-T is too short to calculate the diffusivity.

	SchNet	SchNet-GPIP	GemNet-T [45]	GemNet-T-GPIP
Force	9.5	8.4	5.0	3.0
Stability	232 ₍₅₉₎	235 ₍₃₀₎	6 ₍₇₎	25 ₍₃₎
RDF _(O,O)	0.63 _(0.04)	0.45 _(0.03)	0.62 _(0.48)	0.42 _(0.22)
RDF _(H,H)	0.30 _(0.02)	0.20 _(0.02)	0.35 _(0.21)	0.25 _(0.25)
RDF _(H,O)	0.57 _(0.04)	0.45 _(0.04)	0.71 _(0.65)	0.55 _(0.27)
Diffusivity	1.90	1.68	-	-

Table 5 Results on Electrolyte dataset. MAEs for energy and force are reported in [eV] and [eV/Å], respectively.

	SchNet	SchNet-GPIP	PaiNN [46]	PaiNN-GPIP	EGNN [17]	EGNN-GPIP
Energy	0.713	0.516	0.572	0.341	1.331	0.599
Force	0.161	0.135	0.106	0.086	0.396	0.168

For GemNet-T, we use 950 and 50 data for training and validation, respectively. The model performances are tested using 10,000 data sampled from the remaining dataset.

High accuracy of force alone is not sufficient for an effective MD simulation [51]. Therefore, we further evaluate the learned MLIPs through ML-based MD simulation with more quantitative metrics. Specifically, we evaluate the accuracy of force, simulation stability [51], and equilibrium statistics including radial distribution function (RDF) and diffusion coefficient. By initializing from 5 randomly sampled testing configurations, we perform 5 simulations of 500 ps with a time step of 1 fs at 300 K temperature. Then the MD trajectories are analyzed to evaluate the MLIPs. As shown in Table 4, GPIP-based MLIPs improve not only the accuracy of force prediction but also other key metrics in MD simulations.

Electrolyte Solutions with PBCs

Electrolyte solutions involve more types of elements and stronger interatomic interactions compared to liquid water. Since the configurational space expands combinatorially while the types of elements increase, training MLIPs for such complex systems is more complicated and attracts more and more attention [9]. The datasets for the electrolyte

solution are generated by CMD simulations on 16 different combinations of solvents and solutes. We have sampled 160,000 configuration from the simulation trajectories for pre-training. For fine-tuning, the forces and energies are calculated using a high-accuracy ab initio method on sampled CMD trajectories with fewer atoms in each sample. Each model is trained on 260 configurations and validated on 40 configurations.

The experimental results on the electrolyte solution datasets are summarized in Table 5. We test the performance of GPIP on various baseline models. Table 5 shows that GPIP significantly improves the performance of MLIPs based on both invariant (SchNet) and equivariant models (PaiNN, and EGNN). Especially, the simplest EGNN benefits the most from GPIP when benchmarked on both force and energy. We also test each task’s effect in GPIP and the results are summarized in Supplementary Material.

3 Conclusion

In this work, we propose GPIP, a novel geometric learning paradigm for MLIPs. GPIP consists of two components: geometric structure generation and geometry-enhanced pre-training. Plenty of 3D geometric structures of various molecular systems can be generated efficiently by performing CMD simulations with empirical force fields. We then design a self-supervised pre-training scheme incorporating three tasks: masking, denoising, and contrastive learning. These tasks aim to capture both topology and spatial structure information from the unlabeled geometric structures produced by CMD simulations. We show that the three tasks are complementary and a single pre-training task may not improve the accuracy significantly. We evaluate our method using various MLIPs and datasets that cover a wide range of molecular systems, from simple molecules to complex systems with PBCs. In addition to the most commonly used MD17, ISO17, and liquid water datasets, we present an electrolyte solution dataset that includes more types of elements and more complex configurations for benchmarking. Our experimental results show that the GPIP-based models consistently and significantly outperform the corresponding baseline models, demonstrating remarkable effectiveness and robustness. The computational costs of GPIP are negligible compared to ab initio calculations to obtain more labeled training data. This work is highly applicable for performing MD simulations using MLIPs, especially for complex molecular systems where sufficient training data is hard to obtain.

4 Methods

4.1 Dataset

Pre-training Dataset.

To obtain sufficient configurations that can cover the test set, we sample a large number of configurations from CMD trajectories to serve as the pre-training datasets. All CMD simulations are conducted with LAMMPS software package[53] and the timestep is set to 1 fs.

For MD17, the pre-training dataset is composed of 160,000 configurations sampled from CMD trajectories performed on eight different organic molecules; and for ISO17,

the CMD simulations are performed on 100 isomers with atoms $C_7O_2H_{10}$, which generates 2,000,000 configurations. These configurations are sampled with time resolution of 1 ps in vacuum at different temperatures varying from 300 K to 1000 K with intervals of 100 K under NVT ensembles, and the force field parameters were taken from OPLS-AA force field [5].

The pre-training dataset for liquid water with PBCs is generated with TIP3P force field parameters [54]. The trajectories contain 64 water molecules and are calculated at 10 different temperatures from 100 K to 1000 K with intervals of 100 K under NVT ensembles and 100,000 configurations are sampled with a resolution of 1 ps. The density of the configurations is determined by AIMD calculation at 1 atm and 300 K with an NPT ensemble.

As for the electrolyte solution pre-training dataset, we select different combinations of ions and solvents to be the initial configurations, which include $[Na]^+$ or $[Li]^+$ cations, $[PF_6]^-$ or $[Tf_2N]^-$ anions, and DME or 1:1 EC+DMC solvent. The mole ratio of ion pairs in the electrolyte solutions is set to be 1 M or 4 M. The force field parameters were taken from OPLS-AA force field [5]. The CMD trajectories on 16 different electrolytes are calculated at temperatures from 100K to 1000K with temperature intervals of 100 K. Each contains 24 (1 M) or 48 (4 M) pairs of ions and 192 (1 M) or 72 (4 M) solvent molecules. The size of the periodic box of each electrolyte solution is determined by a 5 ns simulation with NPT ensemble at 300 K, 1 atm, and an equilibrium stage that anneals the electrolyte solution from 1000 K to 300 K in 10 ns was performed. Eventually, 160,000 configurations of electrolyte solution are sampled with NVT ensemble at different temperatures for 100 ns with a time resolution of 1 ps.

Downstream Dataset.

The MD17 [55], ISO17 [11, 52], and liquid water [56] datasets used for fine-tuning are taken from previous studies. The structures of electrolyte solutions are sampled from 16 CMD trajectories with different compounds and mole ratios whereas the atomic forces and total energies of the solutions were determined by density functional theory (DFT) calculations using PBE exchange-correlation functional[57] and with the Projector Augmented-Wave (PAW) pseudo-potential[58]. A single gamma k-point is used to sample the Brillouin zone and the cutoff energy for the plane-wave-basis set is set to be 400 eV and the electronic self-consistency is considered to be achieved if the change of total energy between two steps is smaller than 10^{-5} eV. Each configuration contains 3 (1 M) or 6 (4 M) pairs of ions and 24 (1 M) or 9 (4 M) solvent molecules. The equilibrium and sampling stages of the fine-tuning data set are identical to the pre-training dataset, and the DFT calculation was performed on randomly selected configurations using the VASP code[58] with a plane-wave basis set. There are in total 800 configurations sampled and calculated.

4.2 Pre-training Settings

After obtaining the pre-training data, we apply three SSL tasks (masking, denoising, and contrastive learning) to learn the spatial and topology information from pre-training data which can be transferred to test data. The final loss function is defined as follows:

$$\mathcal{L}_{\text{final}} = \mathcal{L}_{\text{mask}} + \alpha\mathcal{L}_{\text{denoise}} + \beta\mathcal{L}_{\text{contrast}}, \quad (3)$$

where α and β are hyperparameters for balancing the losses of three tasks: masking, denoising and contrastive learning with corresponding terms $\mathcal{L}_{\text{mask}}$, $\mathcal{L}_{\text{denoise}}$, $\mathcal{L}_{\text{contrast}}$, respectively.

In the pretext task 1, we utilize the cosine error as the criterion for reconstructing original node features. Additionally, we downweight the easy samples in the training set by scaling the cosine error with a power of γ where $\gamma \geq 1$.

$$\mathcal{L}_{\text{mask}} = \frac{1}{|\tilde{N}|} \sum_{i \in \mathcal{C}} \left(1 - \frac{x_i^{0T} x_i^{\text{out}}}{\|x_i^0\| \cdot \|x_i^{\text{out}}\|} \right)^\gamma, \gamma \geq 1, \quad (4)$$

where x_i^0 denotes original feature and x_i^{out} is the output of the decoder, \mathcal{C} is the set of indices of the masked nodes \tilde{N} . The scaling factor γ is the hyper-parameter which can be adjusted according to different datasets.

In the pretext task 2, the GNN model is trained to predict the additional noise under the challenge of randomly masked atoms, and the objective function is

$$\mathcal{L}_{\text{denoise}} = \mathbb{E}_{p(\hat{R}, \tilde{X})} \left[\left\| f_\theta(\tilde{X}, \hat{R}) - \mathcal{E} \right\|_2^2 \right], \quad (5)$$

where f_θ denotes an invariant/equivariant GNN parameterized by θ and $p(\hat{R}, \tilde{X})$ measures the probability distribution of perturbed molecular conformations given the atoms.

In the pretext task 3, the main GNN model is enforced to learn the 3D information from 3D net by maximizing the mutual information between the latent features of these two nets. The corresponding loss function is:

$$\mathcal{L}_{\text{contrast}} = -\frac{1}{n} \sum_{i=1}^n \left[\log \frac{e^{\text{sim}(h_i^a, h_i^b)/\tau}}{\sum_{\substack{k=1 \\ k \neq i}}^N e^{\text{sim}(h_i^a, h_k^b)/\tau}} \right], \quad (6)$$

where $\text{sim}(h^a, h^b) = h^a \cdot h^b / (\|h^a\| \|h^b\|)$ is the cosine similarity. h^a and h^b are latent codes of GNN and 3D net respectively. τ is a hyperparameter that can be seen as the weight for the most similar negative pair.

The pre-training settings are determined according to the dataset during the experiments. For the MD17 dataset, each invariant or equivariant GNN model is trained for 3 epochs with an initial learning rate of 0.001 and a weight decay of 0.01 during pre-training. We set $\alpha = 1$ and $\beta = 1$ in Equation (3). The models are first pre-trained on the CMD data of all molecules and then fine-tuned separately on the labeled data of each molecule. We utilize the Adam optimizer with a batch size of 100. As for the ISO17 dataset, we train the GNN models for 4 epochs with GPIIP. The mask rate and batch size are set to 0.15 and 100, respectively. We set $\alpha = 1$ and $\beta = 0.5$ in Equation (3). The Adam optimizer is utilized with a learning rate of 5×10^{-5} and a weight decay of 0.01.

For the datasets with PBCs, we train the GNN models for 3 epochs with GPIIP. We employed the Adam optimizer with an initial learning rate of 4×10^{-3} and a weight decay of 0.01. Additionally, we set the pre-training loss with $\alpha = 1$ and $\beta = 0.1$ in

Equation (3). The liquid water dataset uses a mask rate of 0.15 and a batch size of 100, while the electrolyte dataset uses a mask rate of 0.05 and a batch size of 3.

4.3 Fine-tuning Settings

All experiments are implemented by PyTorch 1.8.0 with four NVIDIA A100 cards. We construct the loss function to fit the total energy E as well as the forces F_i for each atom:

$$\mathcal{L}_{\text{fine-tune}} = \|E - \hat{E}\|^2 + \frac{100}{n} \sum_{i=0}^n \left\| \mathbf{F}_i - \left(-\frac{\partial \hat{E}}{\partial \mathbf{r}_i} \right) \right\|^2, \quad (7)$$

where n is the total number of atoms in a data sample, \mathbf{r}_i represents the coordinate of atom i , and \hat{E} denotes the predicted energy. The training setup varies when GNNs are trained on different datasets and we show the details as follows.

MD17. The models are trained for 500 epochs. Both training and validation sets consist of 1,000 configurations. The parameters of the pre-trained embedding layers and message-passing layers are transferred during the fine-tuning process. All hyperparameters for each GNN are based on the recommendations from the previous literature [44], and more details regarding the GNNs implemented in this work can be found in Supplementary Material.

ISO17. We utilize two different training sets during fine-tuning: a small dataset of 20,000 configurations and a large dataset with 400,000 configurations. The small dataset is randomly sampled from the large training dataset of 400,000 configurations. For evaluation and test datasets, we follow the splitting strategy reported in the previous literature for ISO17[11]. This makes it convenient for us to evaluate the effectiveness of GPIP. We train the GNN with AdamW [59] optimizer and the hyperparameters are provided in Supplementary Material.

Liquid Water with PBCs. We benchmark different models with training datasets with the sizes of 950 and 9,500 and use the remaining 10,000 structures for testing. We perform 5 simulations of 500 ps by initializing from 5 randomly sampled testing configurations, with a time step of 1 fs, at 300 K temperature, the other experimental settings are the same as [51].

Electrolyte solutions with PBCs. The training set, validation set, and test set contain 240, 60, and 500 configurations respectively. For training hyperparameters, We use the Adam with a learning rate of 5×10^{-4} and a weight decay of 0.8, and train the model for 800 epochs. More details can be seen in Supplementary Material.

Data availability

The data used for pre-training and downstream tasks are available at xxx.

Code availability

The source code for reproducing the findings in this paper are available at xxx.

Acknowledgments

This work is partially supported by the National Key R&D Program of China (No. 2022ZD0160100), and in part by Shanghai Committee of Science and Technology (No. 21DZ1100100).

References

- [1] Hospital, A., Goñi, J.R., Orozco, M., Gelpí, J.L.: Molecular dynamics simulations: advances and applications. *Advances and applications in bioinformatics and chemistry*, 37–47 (2015)
- [2] Senftle, T.P., Hong, S., Islam, M.M., Kylasa, S.B., Zheng, Y., Shin, Y.K., Junkermeier, C., Engel-Herbert, R., Janik, M.J., Aktulga, H.M., *et al.*: The reaxff reactive force-field: development, applications and future directions. *npj Computational Materials* **2**(1), 1–14 (2016)
- [3] Karplus, M., Petsko, G.A.: Molecular dynamics simulations in biology. *Nature* **347**, 631–639 (1990)
- [4] Yao, N., Chen, X., Fu, Z.-H., Zhang, Q.: Applying classical, *Ab Initio*, and machine-learning molecular dynamics simulations to the liquid electrolyte for rechargeable batteries **122**(12), 10970–11021 <https://doi.org/10.1021/acs.chemrev.1c00904>. Accessed 2023-01-17
- [5] Kaminski, G.A., Friesner, R.A., Tirado-Rives, J., Jorgensen, W.L.: Evaluation and reparametrization of the opls-aa force field for proteins via comparison with accurate quantum chemical calculations on peptides. *The Journal of Physical Chemistry B* **105**(28), 6474–6487 (2001)
- [6] Car, R., Parrinello, M.: Unified approach for molecular dynamics and density-functional theory. *Physical review letters* **55**(22), 2471 (1985)
- [7] Butler, K.T., Davies, D.W., Cartwright, H., Isayev, O., Walsh, A.: Machine learning for molecular and materials science **559**(7715), 547–555 <https://doi.org/10.1038/s41586-018-0337-2>. Accessed 2023-02-11
- [8] Noé, F., Tkatchenko, A., Müller, K.-R., Clementi, C.: Machine learning for molecular simulation **71**(1), 361–390 <https://doi.org/10.1146/annurev-physchem-042018-052331>. Accessed 2023-01-17
- [9] Unke, O.T., Chmiela, S., Sauceda, H.E., Gastegger, M., Poltavsky, I., Schütt, K.T., Tkatchenko, A., Müller, K.-R.: Machine learning force fields **121**(16), 10142–10186 <https://doi.org/10.1021/acs.chemrev.0c01111>. Accessed 2023-01-17
- [10] Gilmer, J., Schoenholz, S.S., Riley, P.F., Vinyals, O., Dahl, G.E.: Neural message passing for quantum chemistry. In: *International Conference on Machine Learning*,

- pp. 1263–1272 (2017). PMLR
- [11] Schütt, K., Kindermans, P.-J., Sauceda Felix, H.E., Chmiela, S., Tkatchenko, A., Müller, K.-R.: Schnet: A continuous-filter convolutional neural network for modeling quantum interactions. *Advances in neural information processing systems* **30** (2017)
 - [12] Gasteiger, J., Groß, J., Günnemann, S.: Directional message passing for molecular graphs. *arXiv preprint arXiv:2003.03123* (2020)
 - [13] Thomas, N., Smidt, T., Kearnes, S., Yang, L., Li, L., Kohlhoff, K., Riley, P.: Tensor field networks: Rotation-and translation-equivariant neural networks for 3d point clouds. *arXiv preprint arXiv:1802.08219* (2018)
 - [14] Batzner, S., Musaelian, A., Sun, L., Geiger, M., Mailoa, J.P., Kornbluth, M., Molinari, N., Smidt, T.E., Kozinsky, B.: E (3)-equivariant graph neural networks for data-efficient and accurate interatomic potentials. *Nature communications* **13**(1), 2453 (2022)
 - [15] Villar, S., Hogg, D.W., Storey-Fisher, K., Yao, W., Blum-Smith, B.: Scalars are universal: Equivariant machine learning, structured like classical physics. *Advances in Neural Information Processing Systems* **34**, 28848–28863 (2021)
 - [16] Schütt, K., Unke, O., Gastegger, M.: Equivariant message passing for the prediction of tensorial properties and molecular spectra. In: *International Conference on Machine Learning*, pp. 9377–9388 (2021). PMLR
 - [17] Satorras, V.G., Hoogeboom, E., Welling, M.: E (n) equivariant graph neural networks. In: *International Conference on Machine Learning*, pp. 9323–9332 (2021). PMLR
 - [18] Velickovic, P., Fedus, W., Hamilton, W.L., Liò, P., Bengio, Y., Hjelm, R.D.: Deep graph infomax. *ICLR (Poster)* **2**(3), 4 (2019)
 - [19] Hassani, K., Khasahmadi, A.H.: Contrastive multi-view representation learning on graphs. In: *International Conference on Machine Learning*, pp. 4116–4126 (2020). PMLR
 - [20] Qiu, J., Chen, Q., Dong, Y., Zhang, J., Yang, H., Ding, M., Wang, K., Tang, J.: Gcc: Graph contrastive coding for graph neural network pre-training. In: *Proceedings of the 26th ACM SIGKDD International Conference on Knowledge Discovery & Data Mining*, pp. 1150–1160 (2020)
 - [21] Hu, W., Liu, B., Gomes, J., Zitnik, M., Liang, P., Pande, V., Leskovec, J.: Strategies for pre-training graph neural networks. *arXiv preprint arXiv:1905.12265* (2019)
 - [22] You, Y., Chen, T., Wang, Z., Shen, Y.: When does self-supervision help graph

- convolutional networks? In: International Conference on Machine Learning, pp. 10871–10880 (2020). PMLR
- [23] Hou, Z., Liu, X., Cen, Y., Dong, Y., Yang, H., Wang, C., Tang, J.: Graphmae: Self-supervised masked graph autoencoders. In: Proceedings of the 28th ACM SIGKDD Conference on Knowledge Discovery and Data Mining, pp. 594–604 (2022)
 - [24] Chen, H., Zhang, S., Xu, G.: Graph masked autoencoder. arXiv preprint arXiv:2202.08391 (2022)
 - [25] Kipf, T.N., Welling, M.: Variational graph auto-encoders. arXiv preprint arXiv:1611.07308 (2016)
 - [26] Kingma, D.P., Welling, M.: Auto-encoding variational bayes. arXiv preprint arXiv:1312.6114 (2013)
 - [27] Zhou, G., Gao, Z., Ding, Q., Zheng, H., Xu, H., Wei, Z., Zhang, L., Ke, G.: Uni-mol: A universal 3d molecular representation learning framework (2023)
 - [28] Liu, S., Guo, H., Tang, J.: Molecular geometry pretraining with se (3)-invariant denoising distance matching. arXiv preprint arXiv:2206.13602 (2022)
 - [29] Sun, K., Lin, Z., Zhu, Z.: Multi-stage self-supervised learning for graph convolutional networks on graphs with few labeled nodes. In: Proceedings of the AAAI Conference on Artificial Intelligence, vol. 34, pp. 5892–5899 (2020)
 - [30] Zhu, Y., Xu, Y., Yu, F., Wu, S., Wang, L.: Cagmn: Cluster-aware graph neural networks for unsupervised graph representation learning. arXiv preprint arXiv:2009.01674 (2020)
 - [31] Jin, W., Derr, T., Wang, Y., Ma, Y., Liu, Z., Tang, J.: Node similarity preserving graph convolutional networks. In: Proceedings of the 14th ACM International Conference on Web Search and Data Mining, pp. 148–156 (2021)
 - [32] Jin, W., Derr, T., Liu, H., Wang, Y., Wang, S., Liu, Z., Tang, J.: Self-supervised learning on graphs: Deep insights and new direction. arXiv preprint arXiv:2006.10141 (2020)
 - [33] Peng, Z., Dong, Y., Luo, M., Wu, X.-M., Zheng, Q.: Self-supervised graph representation learning via global context prediction. arXiv preprint arXiv:2003.01604 (2020)
 - [34] You, Y., Chen, T., Sui, Y., Chen, T., Wang, Z., Shen, Y.: Graph contrastive learning with augmentations. *Advances in neural information processing systems* **33**, 5812–5823 (2020)
 - [35] You, Y., Chen, T., Shen, Y., Wang, Z.: Graph contrastive learning automated. In: International Conference on Machine Learning, pp. 12121–12132 (2021). PMLR

- [36] Wang, Y., Wang, J., Cao, Z., Barati Farimani, A.: Molecular contrastive learning of representations via graph neural networks. *Nature Machine Intelligence* **4**(3), 279–287 (2022)
- [37] Li, S., Zhou, J., Xu, T., Dou, D., Xiong, H.: Geomgcl: Geometric graph contrastive learning for molecular property prediction. In: *Proceedings of the AAAI Conference on Artificial Intelligence*, vol. 36, pp. 4541–4549 (2022)
- [38] Liu, S., Wang, H., Liu, W., Lasenby, J., Guo, H., Tang, J.: Pre-training molecular graph representation with 3d geometry. In: *International Conference on Learning Representations*
- [39] Stärk, H., Beaini, D., Corso, G., Tossou, P., Dallago, C., Günnemann, S., Liò, P.: 3d infomax improves gnns for molecular property prediction. In: *International Conference on Machine Learning*, pp. 20479–20502 (2022). PMLR
- [40] Zhang, D., Bi, H., Dai, F.-Z., Jiang, W., Zhang, L., Wang, H.: Dpa-1: Pretraining of attention-based deep potential model for molecular simulation. *arXiv preprint arXiv:2208.08236* (2022)
- [41] Wang, Y., Xu, C., Li, Z., Farimani, A.B.: Denoise pre-training on non-equilibrium molecules for accurate and transferable neural potentials. *arXiv preprint arXiv:2303.02216* (2023)
- [42] Chanussot, L., Das, A., Goyal, S., Lavril, T., Shuaibi, M., Riviere, M., Tran, K., Heras-Domingo, J., Ho, C., Hu, W., *et al.*: Open catalyst 2020 (oc20) dataset and community challenges. *Acs Catalysis* **11**(10), 6059–6072 (2021)
- [43] Smith, J.S., Isayev, O., Roitberg, A.E.: Ani-1: an extensible neural network potential with dft accuracy at force field computational cost. *Chemical science* **8**(4), 3192–3203 (2017)
- [44] Liu, Y., Wang, L., Liu, M., Lin, Y., Zhang, X., Oztekin, B., Ji, S.: Spherical message passing for 3d molecular graphs. In: *International Conference on Learning Representations (ICLR)* (2022)
- [45] Gasteiger, J., Becker, F., Günnemann, S.: Gemnet: Universal directional graph neural networks for molecules. *Advances in Neural Information Processing Systems* **34**, 6790–6802 (2021)
- [46] Schütt, K., Unke, O., Gastegger, M.: Equivariant message passing for the prediction of tensorial properties and molecular spectra. In: *International Conference on Machine Learning*, pp. 9377–9388 (2021). PMLR
- [47] Rappé, A.K., Casewit, C.J., Colwell, K., Goddard III, W.A., Skiff, W.M.: Uff, a full periodic table force field for molecular mechanics and molecular dynamics simulations. *Journal of the American chemical society* **114**(25), 10024–10035

(1992)

- [48] He, K., Chen, X., Xie, S., Li, Y., Dollár, P., Girshick, R.: Masked autoencoders are scalable vision learners. In: Proceedings of the IEEE/CVF Conference on Computer Vision and Pattern Recognition, pp. 16000–16009 (2022)
- [49] Vincent, P., Larochelle, H., Bengio, Y., Manzagol, P.-A.: Extracting and composing robust features with denoising autoencoders. In: Proceedings of the 25th International Conference on Machine Learning, pp. 1096–1103 (2008)
- [50] Chmiela, S., Tkatchenko, A., Sauceda, H.E., Poltavsky, I., Schütt, K.T., Müller, K.-R.: Machine learning of accurate energy-conserving molecular force fields. *Science advances* **3**(5), 1603015 (2017)
- [51] Fu, X., Wu, Z., Wang, W., Xie, T., Keten, S., Gomez-Bombarelli, R., Jaakkola, T.: Forces are not enough: Benchmark and critical evaluation for machine learning force fields with molecular simulations. *arXiv preprint arXiv:2210.07237* (2022)
- [52] Ramakrishnan, R., Dral, P.O., Rupp, M., Von Lilienfeld, O.A.: Quantum chemistry structures and properties of 134 kilo molecules. *Scientific data* **1**(1), 1–7 (2014)
- [53] Thompson, A.P., Aktulga, H.M., Berger, R., Bolintineanu, D.S., Brown, W.M., Crozier, P.S., Veld, P.J., Kohlmeyer, A., Moore, S.G., Nguyen, T.D., *et al.*: Lammmps—a flexible simulation tool for particle-based materials modeling at the atomic, meso, and continuum scales. *Computer Physics Communications* **271**, 108171 (2022)
- [54] Jorgensen, W.L., Chandrasekhar, J., Madura, J.D., Impey, R.W., Klein, M.L.: Comparison of simple potential functions for simulating liquid water. *The Journal of chemical physics* **79**(2), 926–935 (1983)
- [55] Bogojeski, M., Vogt-Maranto, L., Tuckerman, M.E., Müller, K.-R., Burke, K.: Quantum chemical accuracy from density functional approximations via machine learning. *Nature communications* **11**(1), 5223 (2020)
- [56] Zhang, L., Han, J., Wang, H., Car, R., Weinan, E.: Deep potential molecular dynamics: a scalable model with the accuracy of quantum mechanics. *Physical review letters* **120**(14), 143001 (2018)
- [57] Perdew, J.P., Burke, K., Ernzerhof, M.: Generalized gradient approximation made simple. *Physical review letters* **77**(18), 3865 (1996)
- [58] Blöchl, P.E.: Projector augmented-wave method. *Physical review B* **50**(24), 17953 (1994)
- [59] Loshchilov, I., Hutter, F.: Decoupled weight decay regularization. *arXiv preprint arXiv:1711.05101* (2017)